IEEE Access
Multidisciplinary | Rapid Review | Open Access Journal

Received 26 September 2022, accepted 12 October 2022, date of publication 28 October 2022, date of current version 4 November 2022.

Digital Object Identifier 10.1109/ACCESS.2022.3217915

RESEARCH ARTICLE

Interference Distribution for Directional Beamforming Mobile Networks

AYMAN T. ABUSABAH, (Graduate Student Member, IEEE), AND RODOLFO OLIVEIRA, (Senior Member, IEEE)

Departamento de Engenharia Electrotécnica e de Computadores, Faculdade de Ciências e Tecnologia—FCT, Universidade NOVA de Lisboa, 2829-516 Caparica, Portugal
Instituto de Telecomunicações, 1049-001 Lisbon, Portugal

Corresponding author: Ayman T. Abusabah (a.sabah@campus.fct.unl.pt)

This work was supported in part by the European Union's Horizon 2020 Research and Innovation Programme under the Marie Skłodowska-Curie European Training Network (ETN) New RAN TEchniques for 5G UltrA-dense Mobile networks (TeamUp5G) under Grant 813391, and in part by the Fundação para a Ciência e Tecnologia under Project UIDB/50008/2020.

ABSTRACT In this paper, we model the aggregate interference power in directional beamforming mobile networks. The work considers the random waypoint model to describe the mobility of the nodes and adopts directional beamforming for communication. The major contribution of this paper is the statistical characterization of the aggregate interference caused by directional beamforming transmissions of mobile interferers to a given node positioned at a reference point. The analysis assumes Rayleigh and Rician small-scale fading channels, a distance-based path-loss large-scale fading model, and a three gain levels sectored antenna model. The quality of the proposed approximations has been confirmed through various simulations for different mobility scenarios, channel conditions, and beamforming parameters, highlighting the effect of directional communications along with mobility on aggregate interference. To demonstrate the practical application of the work, we use two different estimators for the interference characterization. The results confirm the effectiveness of the estimators even when adopting a small set of samples.

INDEX TERMS Interference characterization, directional beamforming, stochastic geometry modeling.

I. INTRODUCTION

Recent progress on physical-layer (PHY) communication technologies allows unprecedented throughput gains through the simultaneous reception of multiple packets including multi-user multiple input multiple output (MU-MIMO) schemes [1] and orthogonal coding schemes, such as Zadoff Chu sequences [2]. In such systems, the nodes simultaneously transmit over the same band and may cause interference to a given receiver, usually the basestation (BS), while decoding a packet transmitted by a specific node. This paradigm shift in the receiver's capability requires knowledge about the stochastic properties of the interference to achieve higher capacity performance or simply to model its performance.

In the context of 5G, the reception of multiple packets simultaneously decoded at the receiver has been explored to support Machine-Type Communications (MTC), where a transmitting device randomly selects one of the 64 orthogonal preambles available per cell and transmits it to the BS in the Physical Random Access Channel (PRACH) [3]. For beyond 5G networks, Massive Ultra-Reliable and Low-Latency Communications (mURLLC) are currently under development for ultra-dense 6G network scenarios to support the access of a massive number of IoT devices [4]. For mURLLC systems, the nodes access the channel in the so-called grant-free mode, meaning that a high number of nodes can simultaneously transmit its preamble to PRACH causing interference to each other. The main motivation for this work is the scenario where multiple mobile transmitters can randomly transmit their signals so that the interference caused to the BS can be characterized, which is of high importance to characterize the performance of massive MTC and mURLLC schemes under development.

Additionally, it is well known that beyond 5G communications will massively rely on directional communications to explore the advantages of high-frequency bands.

The associate editor coordinating the review of this manuscript and approving it for publication was Angel F. García-Fernández.

Directional communications can mitigate the highly imposed isotropic path loss at high-frequency bands. Basically, the nodes can focus their radiation patterns toward a particular spatial direction which reduces the incurred interference [5], and therefore improves spatial reuse. However, the adoption of directional communication has changed the traditional assumption of Gaussian distributed interference due to the existence of dominant interferers. Therefore, the study of the spatial interference statistics in directional networks is crucial as it requires simplified resource allocation and interference management mechanisms when compared to classical communication techniques.

In general, advanced stochastic geometry techniques [6] are widely used to model aggregate interference. Such models usually consider the spatial positions of interfering nodes and their individual radio channel conditions to determine the amount of interference caused to a specific node [7]. The nodes' mobility can introduce a degree of uncertainty for the nodes' position. However, it is a more practical and feasible scenario to be considered when modeling the interference. Therefore, this work characterizes the interference power caused by multiple interferers to a single node considering the mobility of the nodes, the directional communication capability, and the radio propagation channel conditions.

A. RELATED WORKS

Because of its importance in several applications, such as network optimization [8], spectrum sensing [9], localization [10], and others [11], [12], the interference characterization in wireless networks has received increased attention over the last years. Frequently, the central limit theorem (CLT) applies for interference modeling due to a high number of nodes. However, the dominant interferers cause a non-negligible error when CLT is adopted [13]. This has motivated several works to characterize the interference with non-Gaussian models.

Mainly, the complexity of non-Gaussian modeling approaches has limited the researchers' efforts in modeling the aggregate interference in mobile networks. To the best of authors' knowledge, only few and very recent works have considered the interference modeling based on statistics related with interferers mobility [14], [15], [16], [17], [18], [19]. In [14], the aggregate interference is characterized considering multiple static nodes and a single mobile node moves according to a random pattern for the uplink channel. This in turn produces variation in the displacement over time with respect to the location of the nodes. The Random Direction (RD) model is used in [15] to describe the movement of the nodes. The authors characterize the aggregate interference using the probability density function (PDF) of the distance between any pair of nodes. The work in [16] proposed a general-order linear model for node mobility to investigate interference prediction in a mobile ad hoc network. The work in [17] adopted the random waypoint (RWP) mobility model [20] for aggregate interference characterization of multiple mobile nodes only considering the path-loss effect. The work in [18] extends the work in [17] to consider slow fading and fast fading effects. The authors in [19] investigated the impact of wireless powered communications considering mobile nodes moving according to the RWP mobility model.

The adoption of directional communications substantially reduces the interference between the communicating nodes, thus, the multi-user interference becomes no more the major constraint of the network capacity. This has motivated several works to investigate the interference effect on the performance of directional networks [21], [22], [23], [24], [25], [26]. The analysis done in [21] highlights that directional networks can experience a considerable transitional behaviour from a noise-limited regime to an interference-limited one that may effectively reduce throughput/delay performance of the network, which requires adopting proper resource allocation procedures. The authors in [22] investigated the effect of directional beamforming on the medium access control (MAC) design. The work in [23] derived closed-form formulas for computing the coverage probability and the average rate when considering realistic path-loss and blockage models adopting directional communications. Moreover, the work in [24] introduced a model that captures the effects of beamwidth and orientation errors on the throughput in directional wireless Poisson networks. The works in [25] and [26] analysed the distribution of the aggregate interference, and the outage probability in directional networks considering static interferers, respectively. The next section elaborates on the main contributions of this paper.

B. MAIN CONTRIBUTIONS

This work adopts a non-Gaussian modeling approach to characterize the aggregate interference of nodes distributed over an annular region. We assume that the nodes move based on the RWP model introduced in [20] and communicate using directional beamforming through a three gain levels sectored antenna model. The main contributions of this work can be summarized as follows:

- Differently from [14], [15], [16], [17], and [18] where omnidirectional communication is assumed, this work considers the directional communication capability of nodes for the interference characterization.
- While the works in [21], [22], [23], [24], [25], and [26] do not assume any mobility scenario for the analysis of directional communications, the interference modeling in this work adopts the RWP model to describe the nodes' mobility.
- A three gain levels sectored antenna model is presented for directional beamforming. The model is more realistic than other approaches proposed so far [23], [24], [27], [28] and allows a more detailed description of the beams' gain.
- Departing from the fact that inhomogeneous spatial Poisson process (IPP) can characterize the nodes' mobility moving according to the RWP model, we divide the

spatial region into multiple annuli showing that the interferers' density in each annulus can then be approximated by homogeneous Poisson processes with corresponding densities. Then, we drive the moment generation function (MGF) considering distance-based path loss for large-scale fading, Rayleigh and Rician channels for small-scale fading, and directional beamforming.
- We approximate the aggregate interference by the Generalized Extreme Value (GEV) distribution. The GEV distribution parameters are computed by solving a system of equations composed of the raw-moments of the GEV distribution which are obtained from the derived MGF. The simulation results validate the proposed modeling and confirm that the GEV distribution can effectively characterize the aggregate interference.
- We enrich the work and demonstrate its practical value by adopting two different estimators for the estimation of the GEV parameters, namely, moment-based estimator and probability weighted moments estimator. Both estimators achieve high accuracy even when a small number of samples is used in the estimation process.

Notations: In this work, $P(X = x)$ represents the probability of the random variable (RV) X, $f_X(\cdot)$ represents the PDF, $F_X(\cdot)$ represents the Cumulative Distribution Function (CDF), $M_X(s)$ represents the MGF defined as $M_X(s) = \mathrm{E}[e^{sX}]$, $\delta(\cdot)$ represents Dirac's delta function, $\Gamma(\cdot)$ is the complete Gamma function, Gamma(k, θ) represents the Gamma distribution with shape k and scale θ, $\mathrm{E}[X]$ denotes the expectation of the RV X, and ${}_2\mathrm{F}_1(a, b, c, z)$ represents the Gauss Hypergeometric function.

II. NETWORK MODEL

The adopted network scenario assumes that n mobile nodes are spread over a spatial area defined by $X_{max} \times Y_{max}$. We adopt the RWP model proposed in [20] and assumed in several works such as [17], [18], and [19], to describe the mobility of the nodes across the network. Initially, the position of every node (x, y) is randomly sampled from the uniform distribution represented by $x \in [0, X_{max}]$ and $y \in [0, Y_{max}]$. Then, the node moves to another random position, which is also uniformly chosen as the starting point, with a velocity v uniformly sampled from $v \in [V_{min}, V_{max}]$. Thereafter, the node remains stopped for a pause time T_p before repeating the same cycle. We denote the nodes' average velocity by $\mathrm{E}[V]$ [20]

$$\mathrm{E}[V] = \frac{\mathrm{E}[S]}{(\mathrm{E}[V_{wp}])^{-1}\mathrm{E}[S] + T_p}, \tag{1}$$

where $\mathrm{E}[V_{wp}] = \left(\frac{V_{max} - V_{min}}{\ln(\frac{V_{max}}{V_{min}})}\right)$ denotes the average nodes velocity when T_p approaches to zero, whereas $\mathrm{E}[S]$ is the average distance between two random positions.

The spatial circular model (SCM) [18] is considered to compute the aggregate interference due to multiple transmitting nodes at a reference node N_o located at position (x_o, y_o), $x_o \in [0, X_{max}]$ and $y_o \in [0, Y_{max}]$, as shown in Fig. 1.

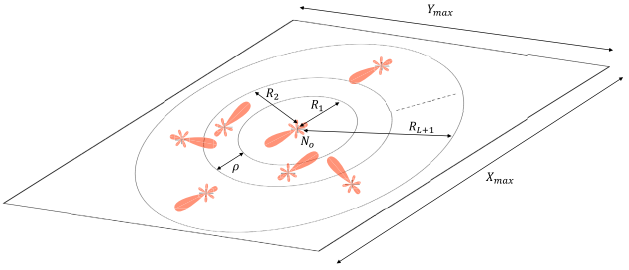

FIGURE 1. A reference node N_o receives interference from n moving transmitters with directional beamforming capability. The inner circle radius is denoted by R_1 while R_{L+1} denotes the outer circle radius.

The SCM admits L annuli where the width of each annulus $l \in \{1, \ldots, L\}$ is represented by ρ. Therefore, the radii of the outer and inner circumferences of the annulus l are given by $R_{l+1} = (R_1 + l\rho)$ and R_l, respectively. Regarding the circular area where the nodes are located, it is simply a composition of a finite number L of annuli areas $A = \sum_{l=1}^{L} A_l$, where $A_l = \pi\left((R_{l+1})^2 - (R_l)^2\right)$ represents the area of the annulus l.

The RV X_l represents the number of nodes located within a specific annulus l which can be approximated by a Poisson process [29], being its truncated probability mass function (PMF) given by [8]

$$P(X_l = k) = \frac{\frac{(\lambda_l A_l \tau)^k}{k!} e^{-\lambda_l A_l \tau}}{\sum_{i=0}^{n} \frac{(\lambda_l A_l \tau)^i}{i!} e^{-\lambda_l A_l \tau}}, \quad k = 0, 1, \cdots, n, \tag{2}$$

where λ_l denotes the nodes' spatial density for the l-th annulus, n represents the number of the nodes distributed over the network, and τ represents the channel access probability depending on the adopted MAC protocol and/or policies, such as the preamble transmission probability in a MTC or mURLLC network. We highlight that the RWP mobility model causes inhomogeneity in the spatial distribution of the nodes. Therefore, the nodes' spatial distribution is approximated by an IPP where λ_l takes different values for each annulus l.

We approximate the spatial PDF of the moving nodes in 2 dimensions, $f_{X,Y}(x, y)$, as given by [20, Th.3]

$$f_{X,Y}(x, y) = \big(p_s f_{init}(x, y) + p_p(1 - p_s) + (1 - p_s)(1 - p_p) f_m(x, y)\big) \times a^{-2}, \tag{3}$$

where p_s is the probability where a node keeps stopped during the whole simulation time, f_{init} is initial spatial distribution of the nodes, $\{X, Y\} \in [0, a]$ in which $a = X_{max} = Y_{max}$, and p_p is the probability that a node is pausing at any random time instant, given by

$$p_p = \frac{(V_{max} - V_{min})T_p}{\ln(\frac{V_{max}}{V_{min}})\mathrm{E}[S] + (V_{max} - V_{min})T_p}. \tag{4}$$

The notation $f_m(x, y)$ represents the asymptotically stationary distribution of the nodes' locations given in [[20], Th.2].

We highlight that the spatial distribution of the moving nodes in (3) considers the characteristics and parameterization of the RWP model. Consequently, the probability that

a moving node is located within the annulus l is written as follows

$$\begin{aligned} P_l &= P(Z_a^l = 1) \\ &= \int_{(x_o-R_{l+1})}^{(x_o+R_{l+1})} \int_{\left(y_o-\sqrt{(R_{l+1})^2-(x-x_o)^2}\right)}^{\left(y_o+\sqrt{(R_{l+1})^2-(x-x_o)^2}\right)} f_{XY}(x,y)\,dy\,dx \\ &\quad - \int_{(x_o-R_l)}^{(x_o+R_l)} \int_{\left(y_o-\sqrt{(R_l)^2-(x-x_o)^2}\right)}^{\left(y_o+\sqrt{(R_l)^2-(x-x_o)^2}\right)} f_{XY}(x,y)\,dy\,dx, \end{aligned} \tag{5}$$

where Z_a^l is a Bernoulli RV representing the hypothetical presence of a node within the l-th annulus. Therefore, the spatial nodes' density of the annulus l can be approximated by the average number of nodes (nP_l) distributed over the area A_l, being given by

$$\lambda_l = \frac{nP_l}{A_l}. \tag{6}$$

Because of the nodes' mobility, λ_l in (6) takes different values within each annulus l where the expected number of nodes positioned within each annulus l is given by the PMF represented in (2). Using the Riemann sum, the area A can be partitioned into a finite number L of small annuli areas that together form the interference region being measured. Therefore, the inhomogeneity of the nodes' density across the whole area A can now be approximated through multiple homogeneous Poisson processes (L) over each partitioned area A_l with a specific corresponding density (λ_l). This methodology has been validated in [18] considering different mobility scenarios. We highlight that the accuracy of the approximation depends mainly on the parameterization of L, which is demonstrated in Section IV.

III. AGGREGATE INTERFERENCE CHARACTERIZATION

The main goal of this work is to characterize the aggregate interference at node N_o due to multiple moving transmitters with directional beamforming capability. The total aggregate interference, I_{agg}, represents the accumulative interference generated by nodes positioned within each annulus with area A_l, as follows

$$I_{agg} = \sum_{l=1}^{L} I_l. \tag{7}$$

Therefore, the distribution of I_l is firstly studied, then, the distribution of I_{agg} is tackled based on the relation in (7).

A. INTERFERENCE OF NODES LOCATED IN THE AREA A_l

Assuming that n_l nodes bounded by the annulus l such that $\sum_{l=1}^{L} n_l = n$, then, the total interference power seen at the reference node N_o from the interferers located in the annulus l, is given by

$$I_l = \sum_{i=1}^{n_l} I_i, \tag{8}$$

where I_i is the interference power of an i-th node which can be expressed by

$$I_i = P_t \psi_i g_i r_l^{-\alpha}, \tag{9}$$

where P_t represents the transmitted power. The small-scale fading channel between the i-th node and the node N_o is represented by ψ_i. The notation $g_i = g_t(\theta_t)g_r(\theta_r)$ denotes the total directivity gain in the i-th node to the N_o node, where $g_t(\theta_t)$ is the gain of the transmitting node and $g_r(\theta_r)$ is the gain of the receiving node, while θ_t and θ_r are the boresight angle directions of the transmitting and receiving antennas, respectively. The distance between the i-th node and the node N_o is represented by r_l, and α is the large-scale path loss coefficient. We highlight that the values ψ_i, g_i, and r_l are instant values of the RVs Ψ_i, G_i, and R_l, respectively.

The total power of the interference caused by the nodes located within annulus l, i.e., within area A_l, represents the sum of each node power. Therefore, the analysis is firstly started by studying the interference power caused by a single node. Based on (9), I_i can be seen as a product between the constant P_t and the RVs Ψ_i, G_i, and $R_i^{-\alpha}$. The following steps are then performed:

1) Given that Ψ_i is a Gamma distributed when considering either Rayleigh or Rician fading [30], we approximate the auxiliary RV Y_i as a ratio between the $P_t\Psi_i$ and R_l^{α}.
2) We find the PDF of G_i, and then, the distribution of I_i is characterized by the product distribution between Y_i and G_i.
3) Finally, the MGF of I_i is derived and, consequently, the MGF of I_l.

1) CHARACTERIZATION OF RANDOM VARIABLE Y_i

We consider the Gamma distribution to describe the power of the fading channel $\Psi_i \sim \text{Gamma}(k_o, \theta_o)$ where k_o and θ_o are the shape and scale parameters, respectively. The Gamma distribution can effectively approximate the stochastic power fading when there is no line-of-sight (LoS) as in the Rayleigh fading channel [25], or the LoS link as in the Rician fading channel [31]. The assumption of small-scale fading is of particular interest when directional beamforming is not implemented with a high number of antennas and the channel hardening condition [32] does not hold, but the proposed model can also accommodate channel hardening by considering deterministic channels.

If the channel is Rayleigh distributed, i.e., $X \sim Ray(B)$, where B is the scale parameter, the fading power is then drawn from the Exponential distribution with the rate parameter $(\frac{1}{2B^2})$, which can be represented by the Gamma distribution as follows

$$\Psi_i^{Ray} \sim \text{Gamma}\left(k_o = 1, \theta_o = \frac{1}{2B^2}\right). \tag{10}$$

Furthermore, the Rician fading channel can be described through the parameters K and Ω where K represents the ratio between the LoS power component and the non-LoS power

components, and Ω denotes the total power from both components. Consequently, the amplitude of the received signal is characterised by the Rician distribution with parameters $\nu^2 = \frac{K\Omega}{1+K}$ and $\sigma^2 = \frac{\Omega}{2(1+K)}$. The parameter K can be represented in the decibels scale $K_{dB} = 10\log_{10}(K)$. If $X \sim Rice(\nu, \sigma)$, then $(\frac{X}{\sigma})^2$ is a non-central Chi-squared distributed with non-centrality parameter $(\frac{\nu}{\sigma})^2$ and two degrees of freedom. Consequently, the Gamma distribution [31] can be used to approximate Ψ_i^{Rice} using moment matching as follows

$$\Psi_i^{Rice} \sim \text{Gamma}\left(k_o = \frac{(\nu^2+2\sigma^2)^2}{4\sigma^2(\nu^2+\sigma^2)}, \theta_o = \frac{4\sigma^2(\nu^2+\sigma^2)}{(\nu^2+2\sigma^2)^2}\right). \tag{11}$$

By definition, if $X \sim \text{Gamma}(k, \theta)$ and $c > 0$, $cX \sim \text{Gamma}(k, c\theta)$, therefore

$$P_i = P_t\Psi_i \sim Gamma(k_o, \vartheta), \tag{12}$$

where $\vartheta = P_t\theta_o$ represents the scale and k_o represents the shape. Assuming that $Q_l = R_l^{\alpha}$, then, we define Y_i as follows

$$Y_i = \frac{P_i}{Q_l}. \tag{13}$$

The probability that an interfering node is located within an annulus l is given by the quotient between the area of the annuli with outer radius r and the annulus area A_l, being represented by the CDF in (14a), which yields to the PDF in (14b) as follows

$$F_{R_l}(r) = \frac{r^2-(R_l)^2}{(R_{l+1})^2-(R_l)^2}, R_l \le r \le R_{l+1}, \tag{14a}$$

$$f_{R_l}(r) = \frac{2r}{(R_{l+1})^2-(R_l)^2}, R_l \le r \le R_{l+1}. \tag{14b}$$

As a result, the CDF and PDF of Q_l are respectively given by (15a) and (15b)

$$F_{Q_l}(q) = \frac{q^{\frac{2}{\alpha}}-(R_l)^2}{(R_{l+1})^2-(R_l)^2}, (R_l)^{\alpha} \le q \le (R_{l+1})^{\alpha}, \tag{15a}$$

$$f_{Q_l}(q) = \frac{2q^{\frac{2}{\alpha}-1}}{\alpha\left((R_{l+1})^2-(R_l)^2\right)}, (R_l)^{\alpha} \le q \le (R_{l+1})^{\alpha}. \tag{15b}$$

Given that the RV Ψ_i is independent of the RV Q_l, then, we use the ratio distribution to derive the PDF of Y_i as follows

$$f_{Y_i}(y) = \int_{-\infty}^{\infty} |q| f_{P_i}(qy) f_{Q_l}(q)\, dq, \tag{16}$$

which can be solved by substituting $f_{Q_l}(q)$ by (15b) and $f_{P_i}(qy)$ by (12), yielding to

$$f_{Y_i}(y) = \int_{(R_l)^{\alpha}}^{(R_{l+1})^{\alpha}} |q| \frac{(qy)^{k_o-1}e^{\frac{-qy}{\vartheta}}}{\Gamma(k_o)(\vartheta)^{k_o}} \frac{2q^{\frac{2}{\alpha}-1}}{\alpha\left((R_{l+1})^2-(R_l)^2\right)}\, dq. \tag{17}$$

Solving the integral in (17) yields to

$$f_{Y_i}(y) = \left(\Gamma\left[k_o+\frac{2}{\alpha}, \frac{(R_l)^{\alpha}y}{\vartheta}\right] - \Gamma\left[k_o+\frac{2}{\alpha}, \frac{(R_{l+1})^{\alpha}y}{\vartheta}\right]\right) \times \frac{2y^{-\frac{2+\alpha}{\alpha}}(\vartheta)^{\frac{2}{\alpha}}}{\alpha\left((R_{l+1})^2-(R_l)^2\right)\Gamma(k_o)}. \tag{18}$$

2) CHARACTERIZATION OF RANDOM VARIABLE G_i

Generally, the radiating antenna elements result in creating continuous sidelobes with descending power levels. For instance, the first and second sidelobes of a rectangular aperture antenna are -13.26 dB and -17.83 dB, respectively, relative to the peak of the main beam. While the interference caused by the sidelobes is relatively small compared to the main lobe, its effect becomes remarkable in the case of concurrent transmissions.

Because of its simplicity, the sectored antenna model with two beams (one main lobe and one sidelobe) has been adopted in several works [23], [24], [27], [28] to approximate the directionality of nodes' communication. Although the two beams approximation does not represent the actual array pattern as it just considers the first sidelobe power, it has been widely adopted mainly for mathematical tractability.

With the traditional two beams sectored antenna model, two levels of gain are assumed, the main lobe gain radiated over its main beamwidth and the sidelobe gain fixed and radiated over the rest of the angular space. With this assumption, the captured/sensed interference could be greater than its real value. While the gain levels of the sidelobes are relatively small compared to the main lobe, they generate a cumulative effect at the receiver side especially in case of high-density scenarios. Therefore, we introduce a more realistic beamforming approximation that brings out the physical properties of directional communications by considering power decaying of the sidelobes over the angular space. The proposed approximation adopts one main lobe and two sidelobes with corresponding gain levels and beamwidths. The model has been assessed through different simulation parameters as presented in Section IV.

We assume that all nodes are equipped with antenna arrays to perform directional beamforming. We adopt a sectored antenna model with multi-beams (one main lobe and two back lobes) as shown in Fig. 2, to represent the gain patterns $g_t(\theta_t)$ and $g_r(\theta_r)$ as follows

$$g_{t,r}(\theta_{t,r}) = \begin{cases} G_1, & \frac{-\omega_1}{2} \le \theta_{t,r} \le \frac{\omega_1}{2} \\ G_2, & -\frac{\omega_1+\omega_2}{2} \le \theta_{t,r} \le -\frac{\omega_1}{2}, \frac{\omega_1}{2} \le \theta_{t,r} \le \frac{\omega_1+\omega_2}{2} \\ G_3, & -\pi \le \theta_{t,r} \le -\frac{\omega_1+\omega_2}{2}, \frac{\omega_1+\omega_2}{2} \le \theta_{t,r} \le \pi. \end{cases} \tag{19}$$

To obtain a more realistic beam pattern, the proposed beamforming model adopts multi-level of gains $\{G_1, G_2, G_3\}$ in which $(G_1 > G_2 > G_3)$, defined by corresponding beamwidths $\{\omega_1, \omega_2, \omega_3\}$ in which $\omega_1+\omega_2+\omega_3 = 2\pi$, and the boresight angle direction $\theta \in [-\pi, \pi)$. The array gains $\{G_1, G_2, G_3\}$ are assumed to be constant for all angles within the corresponding beamwidths $\{\omega_1, \omega_2, \omega_3\}$.

Without loss of generality, all nodes are assumed to be on the same horizontal plane and the beam pattern does not

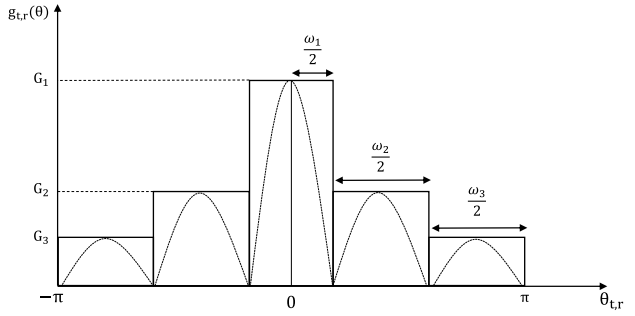

FIGURE 2. Multi-Beams sectored antenna model.

variate over the elevation angle. The orientation of the beams of each node is sampled from the uniform distribution in $[-\pi, \pi)$. As can be noticed, the possible outputs of (19) are G_1, G_2 or G_3 over $[-\pi, \pi)$, thus, the gain distributions, $g_t(\theta_t)$ or $g_r(\theta_r)$, are discrete and their PMF is given by

$$f_{G_{t,r}}(g) = p_1\delta(g - G_1) + p_2\delta(g - G_2) + p_3\delta(g - G_3), \tag{20}$$

where $p_1 = \omega_1/2\pi$, $p_2 = \omega_2/2\pi$, and $p_3 = \omega_3/2\pi$ in which $p_1 + p_2 + p_3 = 1$.

The directivity gain, G_i, is merely a product between the two random gains G_t and G_r, in which the PMF of each one is given by (20). Intuitively, the potential set of outcomes for G_i are $\{G_1^2, G_2^2, G_3^2, G_1G_2, G_1G_3, G_2G_3\}$ with probabilities $\{p_1^2, p_2^2, p_3^2,, 2p_1p_2, 2p_1p_3, 2p_2p_3\}$, respectively. Thus, the PMF of G_i is formulated as follows

$$\begin{aligned} f_{G_i}(g) = {} & p_1^2\delta(g - G_1^2) + p_2^2\delta(g - G_2^2) + p_3^2\delta(g - G_3^2) \\ & + 2p_1p_2\delta(g - G_1G_2) + 2p_1p_3\delta(g - G_1G_3) \\ & + 2p_2p_3\delta(g - G_2G_3). \end{aligned} \tag{21}$$

3) CHARACTERIZATION OF RANDOM VARIABLE I_i

The PDF of the RV I_i can be computed by the product distribution between the RVs Y_i and G_i as follows

$$f_{I_i}(x) = \int_{-\infty}^{\infty} \frac{1}{|g|} f_{G_i}(g) f_{Y_i}(x/g)\, dg, \tag{22}$$

which can be solved by substituting $f_{G_i}(g)$ and $f_{Y_i}(x/g)$ by (21) and (18), respectively, yielding

$$\begin{aligned} f_{I_i}(x) = {} & \frac{p_1^2}{G_1^2} f_{Y_i}\left(\frac{x}{G_1^2}\right) + \frac{p_2^2}{G_2^2} f_{Y_i}\left(\frac{x}{G_2^2}\right) + \frac{p_3^2}{G_3^2} f_{Y_i}\left(\frac{x}{G_3^2}\right) \\ & + \frac{2p_1p_2}{G_1G_2} f_{Y_i}\left(\frac{x}{G_1G_2}\right) + \frac{2p_1p_3}{G_1G_3} f_{Y_i}\left(\frac{x}{G_1G_3}\right) \\ & + \frac{2p_2p_3}{G_2G_3} f_{Y_i}\left(\frac{x}{G_2G_3}\right). \end{aligned} \tag{23}$$

Therefore, the MGF of the interference seen at node N_o due to a single interferer, $M_{I_i}(s) = \mathrm{E}[e^{sI_i}] = \int_{-\infty}^{\infty} e^{sx} f_{I_i}(x)\, dx$, is represented in (24), as shown at the bottom of the next page, where $\varrho(x) = {}_2\mathrm{F}_1(k_o, \frac{-2}{\alpha}, \frac{-2+\alpha}{\alpha}, x)$ is a Gauss Hypergeometric function.

4) CHARACTERIZATION OF RANDOM VARIABLE I_l

Given that I_i's are independent, then for k active interferers, the MGF of the interference power I_l is the product between the MGFs of each I_i, given as follows

$$M_{I_l|k}(s) = M_{I_1}(s) \times M_{I_2}(s) \cdots \times M_{I_k}(s) = \left(M_{I_i}(s)\right)^k. \tag{25}$$

The distribution of the aggregate interference I_l can be then expressed as follows

$$f_{I_l}(j) = \sum_{k=0}^{n} f_{I_l}(j|X_l = k) P(X_l = k). \tag{26}$$

Based on (25), the MFG of I_l can be written as

$$\begin{aligned} \mathrm{E}[e^{sI_l}] &= \sum_{k=0}^{n} P(X_l = k) \int_{-\infty}^{\infty} e^{sj} f_{I_l}(j|X_l = k)\, dj \\ &= \sum_{k=0}^{n} P(X_l = k) M_{I_l|k}(s). \end{aligned} \tag{27}$$

Using (2) and (25), we obtain

$$M_{I_l}(s) = \sum_{k=0}^{n} \frac{(\lambda_l A_l \tau M_{I_i}(s))^k}{k!} e^{-\lambda_l A_l \tau} = e^{\lambda_l A_l \tau (M_{I_i}(s) - 1)}. \tag{28}$$

B. INTERFERENCE OF NODES BOUNDED BY THE AREA A

So far, we have derived the MGF of the interference induced by interferers positioned within the annulus l. Using (7), the MGF of the total aggregate interference caused by interferers bounded by L annuli can be written as follows

$$M_{I_{agg}}(s) = \prod_{l=1}^{L} M_{I_l}(s). \tag{29}$$

Substituting (28) in (29) leads to

$$M_{I_{agg}}(s) = e^{\left(\sum_{l=1}^{L} \lambda_l A_l \tau (M_{I_i}(s) - 1)\right)}. \tag{30}$$

C. DISTRIBUTION OF THE AGGREGATE INTERFERENCE I_{AGG}

In this subsection, we approximate the aggregate interference power I_{agg} by the GEV distribution [33]. To determine the theoretical distributions that achieve the best accuracy in approximating the sample data, the simulated aggregate interference power is used to determine the parameters of different known distributions using the maximum log-likelihood estimation process. The different fit tests presented in Fig. 3 show that the GEV distribution exhibits a close approximation of I_{agg}. A detailed description about the simulation environment parameters can be found in Section IV.

Given that I_{agg} can be approximated by a GEV distribution, then, the PDF and CDF of I_{agg} are given by

$$f_{I_{agg}}(z; \sigma, \gamma, \mu) \approx \frac{1}{\sigma} t(z)^{\gamma+1} e^{-t(z)}, \tag{31a}$$

$$F_{I_{agg}}(z; \sigma, \gamma, \mu) = e^{-t(z)}, \tag{31b}$$

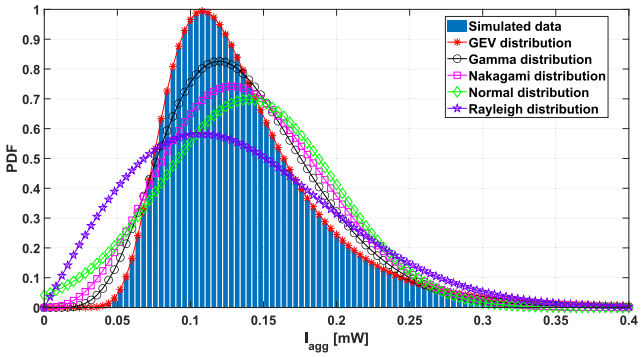

FIGURE 3. Comparison between density of I_{agg} and density of known distributions for a rician fading channel considering $E[V] = 10.82$ m/s, $G_1 = 0$ dB, $G_2 = -7.0$ dB, $G_3 = -10.0$ dB, $\omega_1 = 60°$, $\omega_2 = 200°$, and $\omega_3 = 100°$.

where

$$t(z) = \begin{cases} \left(1 + \gamma(\frac{z-\mu}{\sigma})\right)^{-1/\gamma}, & \gamma \neq 0 \\ e^{-(z-\mu)/\sigma}, & \gamma = 0 \end{cases}. \quad (32)$$

The symbols σ, γ, and μ are the GEV distribution parameters named the scale, shape, and location, respectively. The approximations in (31a) and (31b) require to find the three GEV parameters σ, γ, and μ. Next, we propose an efficient approach for computing the GEV parameters using the raw-moments of I_{agg}.

The proposed approach uses the variance, skewness, and mean of the GEV distribution to set up three equations for σ, γ, and μ, as follows

$$\begin{cases} M_3' = sgn(\gamma)\dfrac{\Gamma(1-3\gamma) - 3\Gamma(1-2\gamma)\Gamma(1-\gamma) + 2\Gamma(1-\gamma)^3}{\left(\Gamma(1-2\gamma) - \Gamma(1-\gamma)\right)^{3/2}}, \\ \qquad\qquad\qquad\qquad\qquad\qquad \gamma < \dfrac{1}{3} \\ M_2' = \dfrac{\sigma^2}{\gamma^2}\left(\Gamma(1-2\gamma) - \Gamma(1-\gamma)^2\right), \quad \gamma < \dfrac{1}{2} \\ M_1 = \mu + \dfrac{\sigma}{\gamma}(\Gamma(1-\gamma) - 1), \quad \gamma < 1, \end{cases} \quad (33)$$

where M_3', M_2', and M_1 are the skewness, variance, and mean of the GEV distribution, respectively. Note that the central moments (skewness and variance) can be written in terms of the raw-moments as follows

$$\begin{cases} M_3' = \dfrac{M_3 - 3M_1(M_2 - M_1^2) - M_1^3}{(M_2 - M_1^2)^{3/2}} \\ M_2' = M_2 - M_1^2, \end{cases} \quad (34)$$

where M_x are the raw-moments of I_{agg}, obtained from (30), i.e., $M_x = \mathrm{E}[I_{agg}^x] = \frac{d^x}{ds^x} M_{I_{agg}}(s)|_{s=0}$.

The first equation in (33) can be numerically solved using *MATHEMATICA* with the *FindRoot* command line or using *MATLAB* with the *vpasolve* command line in an efficient and straightforward manner to obtain γ. Subsequently, the parameters σ and μ are given by

$$\begin{cases} \sigma = \sqrt{\dfrac{\gamma^2(M_2 - M_1^2)}{\Gamma(1-2\gamma) - \Gamma(1-\gamma)^2}} \\ \mu = M_1 - \dfrac{\sigma}{\gamma}(\Gamma(1-\gamma) - 1). \end{cases} \quad (35)$$

D. AGGREGATE INTERFERENCE ESTIMATION

In the previous section, we have characterized the aggregate interference approximated by a GEV distribution. Based on the adopted model, the parameters σ, γ, and μ have been mathematically derived using the raw-moments of I_{agg} in (30). In this subsection, we aim to estimate the parameters of the GEV distribution which could be used in real-time scenarios for the estimation of I_{agg}. Hence, we introduce two estimators for the estimation of σ, γ, and μ using the samples of the aggregate interference collected periodically by the node N_o, namely:

1) Moments Based (MB) Estimator: The MB estimator is based on solving the set of equations in (33) by computing the raw-moments from the collected set of samples represented by $\mathbb{W} = \{W_1, W_2, \cdots, W_m\}$. We also denote the sorted sample set by $W_s = \{W_{1,m}, W_{2,m}, \cdots, W_{m,m}\}$, where $W_{1,m} \leq W_{2,m} \leq \cdots \leq W_{m,m}$. The estimators $(\hat{\sigma}, \hat{\gamma}, \hat{\mu})$ of (σ, γ, μ) only depend on the collected samples and assume no knowledge about the model. Thus, M_1, M_2, and M_3 are estimated though the computation of

$$M_x = \frac{1}{m}\sum_{i=1}^{m}(W_i)^x. \quad (36)$$

2) Probability Weighted Moments (PWM) Estimator: Given a RV D, the weighted moments of D are given by [34]

$$M_{a,b,c} = \mathrm{E}[D^a(F(D))^b(1 - F(D))^c], \quad (37)$$

$$\begin{aligned} M_{I_i}(s) = \frac{1}{(R_{l+1})^2 - (R_l)^2}\Bigg(& (R_{l+1})^2\Big(p_1^2\varrho\left(G_1^2(R_{l+1})^{-\alpha}\vartheta s\right) + p_2^2\varrho\left(G_2^2(R_{l+1})^{-\alpha}\vartheta s\right) + p_3^2\varrho\left(G_3^2(R_{l+1})^{-\alpha}\vartheta s\right) \\ & + 2\,p_1p_2\varrho\left(G_1G_2(R_{l+1})^{-\alpha}\vartheta s\right) + 2\,p_1p_3\varrho\left(G_1G_3(R_{l+1})^{-\alpha}\vartheta s\right) + 2\,p_2p_3\varrho\left(G_2G_3(R_{l+1})^{-\alpha}\vartheta s\right)\Big) \\ & - (R_l)^2\Big(p_1^2\varrho\left(G_1^2(R_l)^{-\alpha}\vartheta s\right) + p_2^2\varrho\left(G_2^2(R_l)^{-\alpha}\vartheta s\right) + p_3^2\varrho\left(G_3^2(R_l)^{-\alpha}\vartheta s\right) + 2\,p_1p_2\varrho\left(G_1G_2(R_l)^{-\alpha}\vartheta s\right) \\ & + 2\,p_1p_3\varrho\left(G_1G_3(R_l)^{-\alpha}\vartheta s\right) + 2\,p_2p_3\varrho\left(G_2G_3(R_l)^{-\alpha}\vartheta s\right)\Big)\Bigg) \end{aligned} \quad (24)$$

TABLE 1. Random waypoint model parameters.

Symbol	Value	Symbol	Value
X_{max}, Y_{max},	1000 m, 1000 m	E[S]	521.4 m [20]
V_{min}	5 m/s	V_{max}	20 m/s
R_1	100 m	ρ	10 m
Simulation time	3000 s	p_s	0
τ	1	L	30

TABLE 2. Beamforming model parameters.

Symbol	Value	Symbol	Value
G_1	0 dB	ω_1	{60°, 45° }
G_2	{-5.2, -7.0, -10.0} dB	ω_2	200°
G_3	{-7.0, -10.0, -13.0} dB	ω_3	{100°, 115° }

TABLE 3. Channel parameters.

Symbol	Value	Symbol	Value
B	1	α	2
K_{dB}	0 dB	Ω	1 Watt
ν	0.707	σ	0.5
P_t	1 W		

where $F(D) = P(D \leq d)$ and $a, b, c \in \mathbb{R}$. In [35], it is shown that $\mathrm{E}[D(F(D))^b]$ can be written as follows

$$M_{1,b,0} = \frac{1}{b+1}\left\{\mu - \frac{\sigma}{\gamma}[1-(b+1)^{\gamma}\Gamma(1-\gamma)]\right\}, \quad (38)$$

for $\gamma < 1$ and $\gamma \neq 0$. A system of equations can be set using (38) as follows

$$\begin{cases} M_{1,10,0} = \mu - \dfrac{\sigma}{\gamma}(1-\Gamma(1-\gamma)) \\ 2M_{1,1,0} - M_{1,0,0} = \dfrac{\sigma}{\gamma}\Gamma(1-\gamma)(2^{\gamma}-1) \\ \dfrac{3M_{1,2,0} - M_{1,0,0}}{2M_{1,1,0} - M_{1,0,0}} = \dfrac{3^{\gamma}-1}{2^{\gamma}-1}. \end{cases} \quad (39)$$

Consequently, the estimators $(\hat{\sigma}, \hat{\gamma}, \hat{\mu})$ of (σ, γ, μ) are the solution of (39), where $M_{1,b,0}$ can be computed by the unbiased estimator presented in [36] as follows

$$\hat{M}_{1,b,0} = \frac{1}{m}\sum_{j=1}^{m}\left(\prod_{l=1}^{b}\frac{j-l}{m-1}\right)W_{j,m}. \quad (40)$$

IV. MODEL EVALUATION

In this section, we use simulation to validate the approximations proposed to model the aggregate interference. The proposed methodology is validated by comparing the numerical results with simulated ones. The RWP model parameters describing the nodes' mobility are presented in Table 1, while the beamforming and channel parameters are listed in Table 2 and Table 3, respectively. To verify the accuracy of the aggregate interference model proposed in this work, we compare the model's numerical results with simulated results

The nodes' mobility was captured during 3000 s considering a square simulation area of (1000m ×1000m). The limits of the nodes' velocity were parameterized to $V_{min} = 5$ m/s and $V_{max} = 20$ m/s in three different mobility scenarios:

TABLE 4. Comparison between the theoretical raw-moments of I_{agg} and the moments computed from simulated data.

	Simulation		
E[V]	10.82 m/s	3.52 m/s	1.5 m/s
M_1	1.34×10^{-4}	1.00×10^{-4}	9.02×10^{-5}
M_2	2.29×10^{-8}	1.25×10^{-8}	1.02×10^{-8}
M_3	4.56×10^{-12}	2.00×10^{-12}	1.50×10^{-12}
	Theoretical		
E[V]	10.82 m/s	3.52 m/s	1.5 m/s
M_1	1.34×10^{-4}	1.00×10^{-4}	9.03×10^{-5}
M_2	2.31×10^{-8}	1.26×10^{-8}	1.03×10^{-8}
M_3	4.64×10^{-12}	2.03×10^{-12}	1.55×10^{-12}

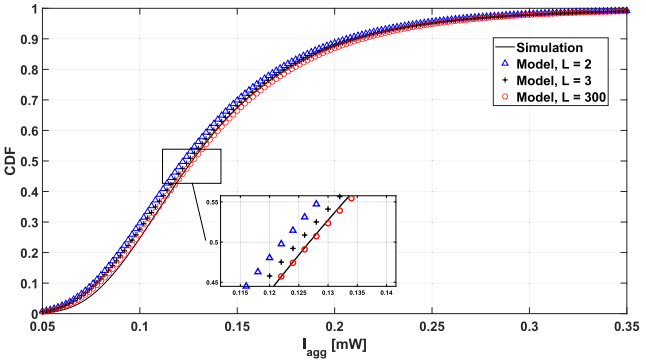

FIGURE 4. CDFs of I_{agg} for a rician fading channel and $L = \{2, 3, 300\}$ considering E[V] = 10.82 m/s, $G_1 = 0$ dB, $G_2 = -7.0$ dB, $G_3 = -10.0$ dB, $\omega_1 = 60°$, $\omega_2 = 200°$, and $\omega_3 = 100°$.

1) Scenario 1: E[V] = 10.82 m/s was defined adopting $T_p = 0$ s.
2) Scenario 2: E[V] = 3.52 m/s was defined adopting $T_p = 100$ s.
3) Scenario 3: E[V] = 1.5 m/s was defined adopting $T_p = 300$ s.

The receiver node N_o was located at $x_o = y_o = 500$ m, i.e., the origin of the simulation area. The aggregate interference samples were collected by the node N_o every second and 3×10^6 realisations were run. The simulation considers $n = 100$ moving nodes and the interference is caused by the nodes located between $R_1 = 100$ m and $R_{L+1} = 400$ m.

Initially, the derived MGF of I_{agg}, $M_{I_{agg}}$, in (30) is verified. Table 4 compares the first, second, and third theoretical raw-moments with the simulated ones for different mobility scenarios. The close matching between the results validates the derived MGF and confirms its effectiveness in computing the moments of I_{agg} that are used to approximate its distribution.

We start by comparing the simulated results with numerical results obtained using different L values as depicted in Fig. 4. Although the results confirm the effectiveness of the proposed modeling when considering $L \leq 3$, the model's accuracy increases with L. This observation can be attributed to the homogeneity distribution of the nodes approached when considering high parameterization of L, which harmonizes with the mathematical approximation derived in (6).

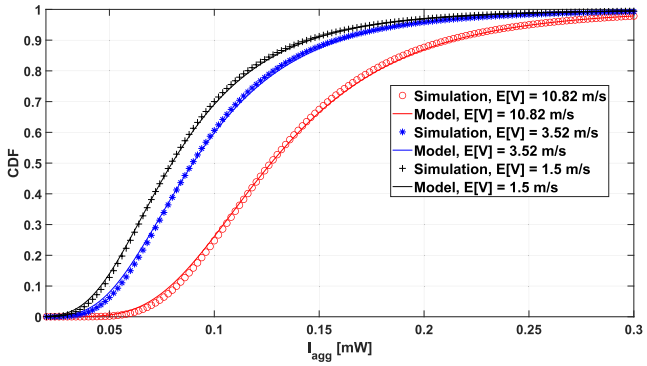

FIGURE 5. CDFs of I_{agg} for a rician fading channel considering different mobility scenarios and parameters $G_1 = 0$ dB, $G_2 = -7.0$ dB, $G_3 = -10.0$ dB, $\omega_1 = 60°$, $\omega_2 = 200°$, and $\omega_3 = 100°$.

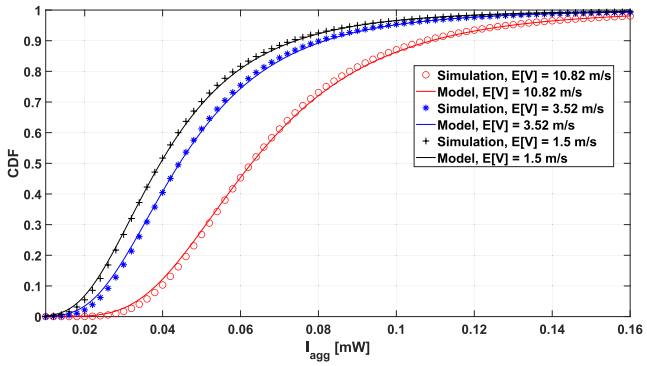

FIGURE 6. CDFs of I_{agg} for a rayleigh fading channel considering different mobility scenarios and parameters $G_1 = 0$ dB, $G_2 = -7.0$ dB, $G_3 = -10.0$ dB, $\omega_1 = 60°$, $\omega_2 = 200°$, and $\omega_3 = 100°$.

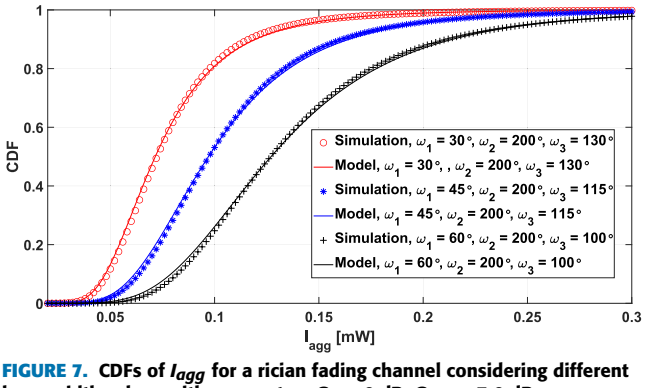

FIGURE 7. CDFs of I_{agg} for a rician fading channel considering different beamwidth values with parameters $G_1 = 0$ dB, $G_2 = -7.0$ dB, $G_3 = -10.0$ dB, and $E[V] = 10.82$ m/s.

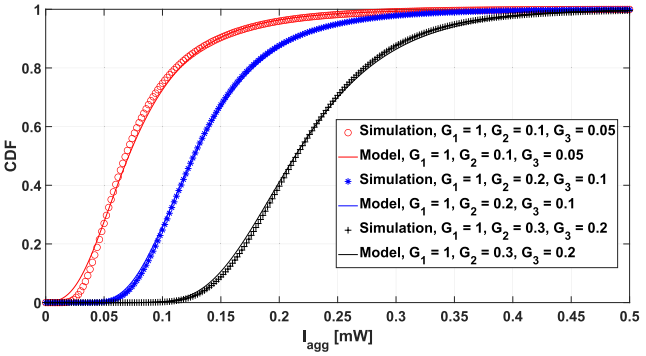

FIGURE 8. CDFs of I_{agg} for a rician fading channel considering different gain levels with parameters $\omega_1 = 60°$, $\omega_2 = 200°$, $\omega_3 = 100°$, and $E[V] = 10.82$ m/s.

Fig. 5 and Fig. 6 illustrate the CDFs of the aggregate interference power for Rician and Rayleigh channels, respectively. The Monte Carlo simulation was used to obtain the "Simulation" curves, whereas the "Model" curves were computed by (31b) considering different mobility scenarios (Scenario 1, Scenario 2, and Scenario 3). The comparison between the results obtained by simulation and the results obtained by the proposed model indicates that the aggregate interference power can be effectively represented by the GEV distribution under the mobility and beamforming assumptions. Moreover, the results show that the increase in the speed of the nodes leads to higher interference power. This can be attributed to the increase of the average number of nodes around N_o for higher average speeds, which is also aligned with the conclusions in [18]. Compared to the results reported in [17], [18], we highlight that the current results show a significant decrease in the aggregate interference power mainly because the channel is established in a specific direction when adopting beamforming.

To assess the proposed beamforming model and highlight its effect on the aggregate interference, the CDFs of I_{agg} are simulated considering different beamwidth values and gain levels. Fig. 7 depicts the CDFs of I_{agg} considering different beamwidths (ω_1, ω_1, and ω_3). The results show that the aggregate interference decreases when narrowing the spatial radiation of the main lobe ($\omega_1 = 30° < \omega_1 = 45° < \omega_1 = 60°$). This can be justified by the fact that the radiating power is more concentrated over smaller spatial regions when narrowing the beams, which eventually limits the interference in the network. This transitional behaviour in the interference highlights the importance of interference characterization for directional beamforming. The limited-interference behaviour requires a design of novel interference avoidance techniques at the MAC layer, taking the advantage of the reduced interference due to directional beamforming.

On the other hand, the side lobes gain effect on the aggregate interference is evaluated considering different side lobes gain levels as represented in Fig. 8. The results show that the aggregate interference increases when adopting higher side lobes gain values $\big((G_2 = 0.3, G_3 = 0.2)$ over $(G_2 = 0.2, G_3 = 0.1)$ and $(G_2 = 0.2, G_1 = 0.1)$ over $(G_2 = 0.1, G_3 = 0.05)\big)$. The results highlight the influence of the side lobes on increasing the aggregate interference power which confirms the compatibility of the adopted beamforming model with different scenarios and parameters.

The accuracy of the proposed estimators (MB and PWM) are assessed in Fig. 9 for the three mobility scenarios (Scenario 1, Scenario 2, Scenario 3). The CDFs of the simulated data are compared with the CDFs computed by estimating the GEV parameters using (36) and (40) for the MB and PWM estimators, respectively. The results indicate a close matching between the simulated CDFs and the CDFs generated with the proposed estimators for a sample set of length $m = 100$. However, the results obtained by the PWM

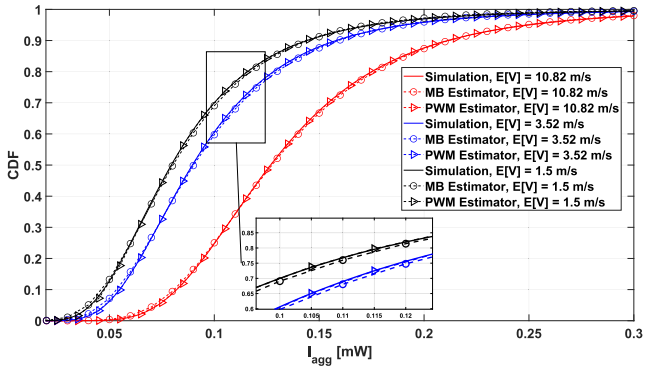

FIGURE 9. CDFs of the estimated I_{agg} through the MB estimator and PWM estimator for $m = 100$ samples considering a rician fading channel.

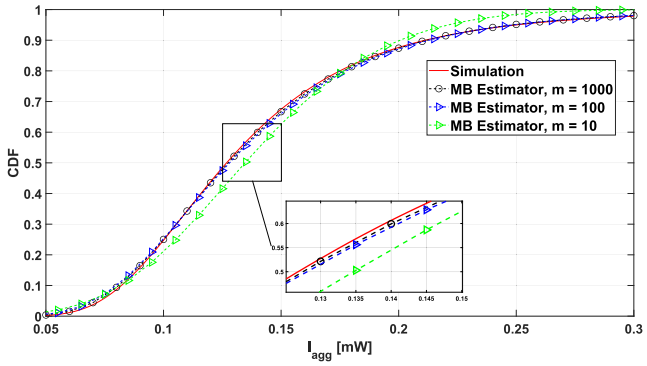

FIGURE 10. CDFs of the estimated I_{agg} through the MB estimator considering different sample set lengths ($m = \{1000, 100, 10\}$) for a rician fading channel and $E[V] = 10.82$ m/s.

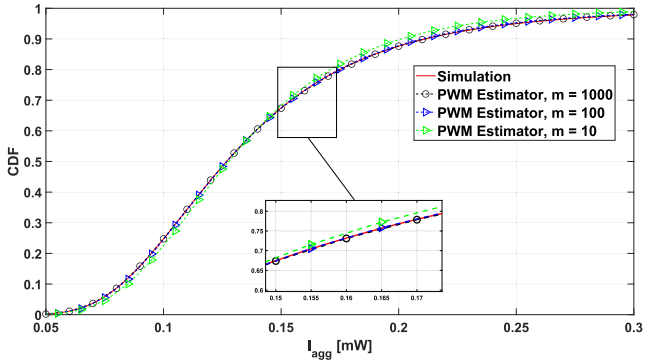

FIGURE 11. CDFs of the estimated I_{agg} through the PWM estimator considering different sample set lengths ($m = \{1000, 100, 10\}$) for a rician fading channel and $E[V] = 10.82$ m/s.

estimator show better accuracy than the ones obtained by the MB estimator, as illustrated in Fig. 9.

To highlight the impact of the sample set length on the estimation quality, the CDFs of I_{agg} considering different sample set lengths ($m = \{1000, 100, 10\}$) for the MB and PWM estimators are plotted in Fig. 10 and Fig. 11, respectively. The simulation adopts the Scenario 1 mobility scenario with the Rician fading channel. The results indicate that the more samples we utilize, the better estimation quality we obtain for both estimators. Moreover, we highlight the high accuracy of both estimators even for a small set of samples length. As a final remark, the PWM estimator seems to be more efficient than the MB estimator when considering small m values.

V. CONCLUSION

In this work, we have characterized the aggregate interference on a reference node caused by mobile users moving according to the RWP mobility model in wireless beamforming networks. The proposed modeling and theoretical derivations have been verified by the comparison with several simulation results. The validation considers large-scale path loss and small-scale fading channels over different beamforming parameters and mobility scenarios, validating the accuracy and effectiveness of the proposed approximations. Compared to previous works, we notice a significant decrease in the aggregate interference power when considering beamforming which requires adequate and innovative MAC schemes with simplified resource allocation and interference management mechanisms. Moreover, we have defined two different estimators for the interference characterization. The results confirmed the estimators' efficiency even when utilizing a small length of samples.

ACKNOWLEDGMENT

The authors would like to thank Luís Irio for the help in the simulations of the mobility scenarios that greatly improved the manuscript.

REFERENCES

[1] K. P. Dasala, J. M. Jornet, and E. W. Knightly, "Scaling mmWave WLANs with single RF chain multiuser beamforming," *IEEE/ACM Trans. Netw.*, early access, Jun. 23, 2022, doi: 10.1109/TNET.2022.3182976.

[2] R.-A. Pitaval, B. M. Popovic, P. Wang, and F. Berggren, "Overcoming 5G PRACH capacity shortfall: Supersets of Zadoff–Chu sequences with low-correlation zone," *IEEE Trans. Commun.*, vol. 68, no. 9, pp. 5673–5688, Sep. 2020.

[3] *Evolved Universal Terrestrial Radio Access (E-UTRA) Physical Channels and Modulation, 3rd Generation Partnership Project (3GPP)*, document (TS) 36.221, Version 13.5.0, 3GPP, 2016.

[4] Y. Liu, Y. Deng, M. Elkashlan, A. Nallanathan, and G. K. Karagiannidis, "Optimization of grant-free NOMA with multiple configured-grants for mURLLC," *IEEE J. Sel. Areas Commun.*, vol. 40, no. 4, pp. 1222–1236, Apr. 2022.

[5] H. Shokri-Ghadikolaei, C. Fischione, G. Fodor, P. Popovski, and M. Zorzi, "Millimeter wave cellular networks: A MAC layer perspective," *IEEE Trans. Commun.*, vol. 63, no. 10, pp. 3437–3458, Oct. 2015.

[6] F. Baccelli and B. Blaszczyszyn, *Stochastic Geometry and Wireless Networks*. Delft, The Netherlands: Now, Sep. 2009.

[7] M. Dong and T. Kim, "Interference analysis for millimeter-wave networks with geometry-dependent first-order reflections," *IEEE Trans. Veh. Technol.*, vol. 67, no. 12, pp. 12404–12409, Dec. 2018.

[8] M. Haenggi and R. K. Ganti, "Interference in large wireless networks," *Found. Trends Netw.*, vol. 3, no. 2, pp. 127–248, Jan. 2009.

[9] A. Rabbachin, T. Q. S. Quek, H. Shin, and M. Z. Win, "Cognitive network interference," *IEEE J. Sel. Areas Commun.*, vol. 29, no. 2, pp. 480–493, Feb. 2011.

[10] M. Z. Win, A. Conti, S. Mazuelas, Y. Shen, W. M. Gifford, D. Dardari, and M. Chiani, "Network localization and navigation via cooperation," *IEEE Commun. Mag.*, vol. 49, no. 5, pp. 56–62, May 2011.

[11] W. Feng, Y. Wang, D. Lin, N. Ge, J. Lu, and S. Li, "When mmWave communications meet network densification: A scalable interference coordination perspective," *IEEE J. Sel. Areas Commun.*, vol. 35, no. 7, pp. 1459–1471, Jul. 2017.

[12] P. Zhou, X. Fang, X. Wang, Y. Long, R. He, and X. Han, "Deep learning-based beam management and interference coordination in dense mmWave networks," *IEEE Trans. Veh. Technol.*, vol. 68, no. 1, pp. 592–603, Jan. 2019.
[13] M. Chiani, "Analytical distribution of linearly modulated cochannel interferers," *IEEE Trans. Commun.*, vol. 45, no. 1, pp. 73–79, Jan. 1997.
[14] S. Yarkan, A. Maaref, K. H. Teo, and H. Arslan, "Impact of mobility on the behavior of interference in cellular wireless networks," in *Proc. IEEE Global Telecommun. Conf. (GLOBECOM)*, Nov. 2008, pp. 1–5.
[15] X. Zhang, L. Wu, Y. Zhang, and D. K. Sung, "Interference dynamics in MANETs with a random direction node mobility model," in *Proc. IEEE Wireless Commun. Netw. Conf. (WCNC)*, Apr. 2013, pp. 3788–3793.
[16] Y. Cong, X. Zhou, and R. A. Kennedy, "Interference prediction in mobile ad hoc networks with a general mobility model," *IEEE Trans. Wireless Commun.*, vol. 14, no. 8, pp. 4277–4290, Aug. 2015.
[17] L. Irio, R. Oliveira, and L. Bernardo, "Aggregate interference in random waypoint mobile networks," *IEEE Commun. Lett.*, vol. 19, no. 6, pp. 1021–1024, Jun. 2015.
[18] L. Irio, A. Furtado, R. Oliveira, L. Bernardo, and R. Dinis, "Interference characterization in random waypoint mobile networks," *IEEE Trans. Wireless Commun.*, vol. 17, no. 11, pp. 7340–7351, Nov. 2018.
[19] L. Irio, R. Oliveira, D. B. da Costa, and M.-S. Alouini, "Impact of wireless-powered communications in coexisting mobile networks," *IEEE Wireless Commun. Lett.*, vol. 9, no. 7, pp. 1060–1064, Jul. 2020.
[20] C. Bettstetter, G. Resta, and P. Santi, "The node distribution of the random waypoint mobility model for wireless ad hoc networks," *IEEE Trans. Mobile Comput.*, vol. 2, no. 3, pp. 257–269, Jul. 2003.
[21] H. Shokri-Ghadikolaei and C. Fischione, "The transitional behavior of interference in millimeter wave networks and its impact on medium access control," *IEEE Trans. Commun.*, vol. 64, no. 2, pp. 723–740, Feb. 2016.
[22] S. Singh, R. Mudumbai, and U. Madhow, "Interference analysis for highly directional 60-GHz mesh networks: The case for rethinking medium access control," *IEEE/ACM Trans. Netw.*, vol. 19, no. 5, pp. 1513–1527, Oct. 2011.
[23] M. Di Renzo, "Stochastic geometry modeling and analysis of multi-tier millimeter wave cellular networks," *IEEE Trans. Wireless Commun.*, vol. 14, no. 9, pp. 5038–5057, Sep. 2015.
[24] J. Wildman, P. H. J. Nardelli, M. Latva-Aho, and S. Weber, "On the joint impact of beamwidth and orientation error on throughput in directional wireless Poisson networks," *IEEE Trans. Wireless Commun.*, vol. 13, no. 12, pp. 7072–7085, Dec. 2014.
[25] A. T. Abusabah and R. Oliveira, "Aggregate interference power characterization for directional beamforming wireless networks," in *Proc. IEEE 93rd Veh. Technol. Conf. (VTC-Spring)*, Apr. 2021, pp. 1–6.
[26] A. T. Abusabah and R. Oliveira, "Outage probability for directional beamforming in high density wireless networks," in *Proc. Int. Wireless Commun. Mobile Comput. (IWCMC)*, Jun. 2021, pp. 709–714.
[27] T. Bai and R. W. Heath, Jr., "Coverage and rate analysis for millimeter-wave cellular networks," *IEEE Trans. Wireless Commun.*, vol. 14, no. 2, pp. 1100–1114, Feb. 2014.
[28] S. Singh, M. N. Kulkarni, A. Ghosh, and J. G. Andrews, "Tractable model for rate in self-backhauled millimeter wave cellular networks," *IEEE J. Sel. Areas Commun.*, vol. 33, no. 10, pp. 2196–2211, Oct. 2015.
[29] A. Papoulis and S. U. Pillai, *Probability-Random Variables and Stochastic Processes*, 4th ed. New York, NY, USA: McGraw-Hill, 2001.
[30] A. Abdi and M. Kaveh, "On the utility of gamma PDF in modeling shadow fading (slow fading)," in *Proc. IEEE 49th Veh. Technol. Conf.*, vol. 3, May 1999, pp. 2308–2312.
[31] A. T. Abusabah, L. Irio, R. Oliveira, and D. B. da Costa, "Approximate distributions of the residual self-interference power in multi-tap full-duplex systems," *IEEE Wireless Commun. Lett.*, vol. 10, no. 4, pp. 755–759, Apr. 2021.
[32] B. M. Hochwald, T. L. Marzetta, and V. Tarokh, "Multiple-antenna channel hardening and its implications for rate feedback and scheduling," *IEEE Trans. Inf. Theory*, vol. 50, no. 9, pp. 1893–1909, Sep. 2004.
[33] L. Wright, G. Muraleedharan, C. G. Soares, and C. Lucas, *Characteristic Moment Generating Functions Generalised Extreme Value Distribution (GEV)*, Jan. 2010, pp. 269–276.
[34] J. A. Greenwood, J. M. Landwehr, N. C. Matalas, and J. R. Wallis, "Probability weighted moments: Definition and relation to parameters of several distributions expressable in inverse form," *Water Resour. Res.*, vol. 15, no. 5, pp. 1049–1054, Oct. 1979.
[35] J. R. M. Hosking, J. R. Wallis, and E. F. Wood, "Estimation of the generalized extreme-value distribution by the method of probability-weighted moments," *Technometrics*, vol. 27, no. 3, pp. 251–261, 1985.
[36] J. M. Landwehr, N. C. Matalas, and J. R. Wallis, "Probability weighted moments compared with some traditional techniques in estimating Gumbel parameters and quantiles," *Water Resour. Res.*, vol. 15, no. 5, pp. 1055–1064, 1979.

AYMAN T. ABUSABAH (Graduate Student Member, IEEE) received the B.S. degree in telecommunication engineering from Yarmouk University, Irbid, Jordan, and the M.S. degree in telecommunication engineering from Medipol University, Istanbul, Turkey. He is currently pursuing the Ph.D. degree in telecommunication engineering with FCT, NOVA University Lisbon, Portugal. His research interests include the design of PHY/MAC architectures for WLANs and future 5G/6G mobile networks. During the Ph.D. study, he joined the TeamUp5G [a European Training Network (ETN)] Project as an Early Stage Researcher (ESR). He benefited from a unique doctoral training programme covering scientific, technical, business aspects, and spent time experimenting his research in real scenarios.

RODOLFO OLIVEIRA (Senior Member, IEEE) received the Licenciatura degree in electrical engineering from the Faculdade de Ciências e Tecnologia (FCT), Universidade NOVA de Lisboa (UNL), Lisbon, Portugal, in 2000, the M.Sc. degree in electrical and computer engineering from the Instituto Superior Técnico, Technical University of Lisbon, in 2003, and the Ph.D. degree in electrical engineering from UNL, in 2009. From 2007 to 2008, he was a Visiting Researcher at the University of Thessaly. From 2011 to 2012, he was a Visiting Scholar at Carnegie Mellon University. He is currently with the Department of Electrical and Computer Engineering, UNL, and is also affiliated as a Senior Researcher with the Instituto de Telecomunicações, where he researches in the areas of wireless communications, computer networks, and computer science. He serves in the Editorial Board of *Ad Hoc Networks* (Elsevier), *ITU Journal on Future and Evolving Technologies* (ITU J-FET), IEEE Open Journal of the Communications Society, and IEEE Communications Letters.